# Physica Status Solidi A: Applications and Materials Science

## Giant reflection coefficient on $Sc_{0.26}Al_{0.74}N$ /polycrystalline-diamond SAW resonators

--Manuscript Draft--

| | |
|---|---|
| **Manuscript Number:** | pssa.201900360R2 |
| **Full Title:** | Giant reflection coefficient on $Sc_{0.26}Al_{0.74}N$ /polycrystalline-diamond SAW resonators |
| **Article Type:** | Original Paper |
| **Section/Category:** | |
| **Keywords:** | Surface Acoustic Wave Devices; Piezoelectric thin films; Thin film heterostructures; Scandium aluminum nitride thin film |
| **Corresponding Author:** | Miguel Sinusia Lozano<br>Intitute for optoelectronic systems and microtechnology, Universidad Politécnica de Madrid<br>Madrid, Comunidad de Madrid SPAIN |
| **Corresponding Author Secondary Information:** | |
| **Corresponding Author's Institution:** | Intitute for optoelectronic systems and microtechnology, Universidad Politécnica de Madrid |
| **Corresponding Author's Secondary Institution:** | |
| **First Author:** | Miguel Sinusia Lozano |
| **First Author Secondary Information:** | |
| **Order of Authors:** | Miguel Sinusia Lozano |
| | Zhuohui Chen |
| | Oliver Williams |
| | Gonzalo F Iriarte |
| **Order of Authors Secondary Information:** | |
| **Abstract:** | Since the first commercialization of surface acoustic wave (SAW) devices, the technology is being steadily developed, improving the device performances without compromising their power handling nor increasing their size and price. In this work, one-port SAW resonators are fabricated on scandium aluminum nitride (Sc0.26Al0.74N)/polycrystalline diamond heterostructures. The SAW propagation properties are studied by using three different piezoelectric thin film thicknesses within the heterostructure. The Rayleigh and Sezawa resonance frequencies are above 1.5 GHz and 2.5 GHz respectively, achieving Sezawa mode reflection coefficients below -50 dB.<br>The polycrystalline diamond substrate was synthesized by microwave plasma chemical vapor deposition (CVD) on top of 500 µm thick Si (001) substrate. The Sc0.26Al0.74N thin films were synthesized by reactive sputtering at nominally room temperature. The thin film composition was analyzed by Rutherford backscattering spectrometry (RBS). The full width at half maximum of the x-ray diffraction (XRD) ω scans below 3º indicate that the synthesized Sc0.26Al0.74N thin films are highly c-axis oriented.<br>The electromechanical coupling coefficient, the quality factor and the dielectric loss parameters are computed by curve fitting the device electrical measurements to the simulation results of a modified Butterworth Van Dyke (mBVD) model implemented in the advance design system (ADS) tool. |
| **Additional Information:** | |
| **Question** | **Response** |
| Please submit a plain text version of your cover letter here. | Since the first commercialization of surface acoustic wave (SAW) devices, the technology is being steadily developed, improving the device performances without |

| | |
|---|---|
| | compromising their power handling nor increasing their size and price. In this work, one-port SAW resonators are fabricated on scandium aluminum nitride (Sc0.26Al0.74N)/polycrystalline diamond heterostructures. The SAW propagation properties are studied by using three different piezoelectric thin film thicknesses within the heterostructure. The Rayleigh and Sezawa resonance frequencies are above 1.5 GHz and 2.5 GHz respectively, achieving Sezawa mode reflection coefficients below -50 dB.<br>The polycrystalline diamond substrate was synthesized by microwave plasma chemical vapor deposition (CVD) on top of 500 µm thick Si (001) substrate. The Sc0.26Al0.74N thin films were synthesized by reactive sputtering at nominally room temperature. The thin film composition was analyzed by Rutherford backscattering spectrometry (RBS). The full width at half maximum of the x-ray diffraction (XRD) ω scans below 3º indicate that the synthesized Sc0.26Al0.74N thin films are highly c-axis oriented.<br>The electromechanical coupling coefficient, the quality factor and the dielectric loss parameters are computed by curve fitting the device electrical measurements to the simulation results of a modified Butterworth Van Dyke (mBVD) model implemented in the advance design system (ADS) tool. |
| Do you or any of your co-authors have a conflict of interest to declare? | No. The authors declare no conflict of interest. |

**Title:** Giant reflection coefficient on $Sc_{0.26}Al_{0.74}N$ /polycrystalline-diamond SAW resonators

*Author(s), and Corresponding Author(s) Miguel Sinusía Lozano, Zhuohui Chen, Oliver A. Williams, Gonzalo F. Iriarte**

((Optional Dedication))

Author 1: PhD. Candidate, Miguel Sinusia Lozano. Author 4: Prof. Dr. Gonzalo Fuentes Iriarte
Institute for optoelectronic systems and microtechnology (ISOM), Universidad Politécnica de Madrid, Madrid, Spain

E-mail: gonzalo.fuentes@upm.es

Author 3: Dr. Zhuohui Chen
Huawei Technologies Co Ltd, Ontario, Canada

Author 4: Prof. Dr. Oliver A. Williams
School of Physics and Astronomy, Cardiff University, United Kingdom

Keywords: Surface acoustic wave devices, Piezoelectric thin films, Thin film heterostructures, Scandium aluminum nitride thin films

Abstract:

Since the first commercialization of surface acoustic wave (SAW) devices, the technology is being steadily developed, improving the device performances without compromising their power handling nor increasing their size and price. In this work, one-port SAW resonators are fabricated on scandium aluminum nitride ($Sc_{0.26}Al_{0.74}N$)/polycrystalline diamond heterostructures. The SAW propagation properties are studied by using three different piezoelectric thin film thicknesses within the heterostructure. The Rayleigh and Sezawa resonance frequencies are above 1.5 GHz and 2.5 GHz respectively, achieving Sezawa mode reflection coefficients below -50 dB.

The polycrystalline diamond substrate was synthesized by microwave plasma chemical vapor deposition (CVD) on top of 500 µm thick Si (001) substrate. The $Sc_{0.26}Al_{0.74}N$ thin films were synthesized by reactive sputtering at nominally room temperature. The thin film composition was analyzed by Rutherford backscattering spectrometry (RBS). The full width at half maximum of the x-ray diffraction (XRD) ω scans below 3º indicate that the synthesized $Sc_{0.26}Al_{0.74}N$ thin films are highly c-axis oriented.

The electromechanical coupling coefficient, the quality factor and the dielectric loss parameters are computed by curve fitting the device electrical measurements to the simulation results of a modified Butterworth Van Dyke (mBVD) model implemented in the advance design system (ADS) tool.

## ((1)) Introduction

Surface acoustic wave (SAW) technologies are widely used in telecommunications. Especially during the last decade, in which the demand of reliable SAW technological solutions has grown exponentially in wireless communication systems. SAW based devices are small, stable, provide high power handling, compatibility with standard integrated circuits manufacturing processes and low-cost production.

Moreover, when the consideration turns into SAW resonators, their performances provide very large quality factors together with low insertion losses [1].

The SAW acoustic velocity (Equation (1)) depends on the elastic modulus ($E$) and density ($\rho$) of the material through which the wave propagates [2].

$$V = \sqrt{E/\rho} \tag{1}$$

However, when the surface acoustic wave is generated with a SAW device which design comprises a stacking of layers (heterostructure), the velocity of the propagating wave is a compromise between the acoustic velocities of the layers through the wave propagates. Thereby, a suitable solution for fabricating SAW devices with high operating frequencies is to design heterostructures comprising a layer with high acoustic velocity. For this, diamond outstands, since it exhibits the highest acoustic velocity. Several studies have reported SAW devices fabricated on heterostructures with diamond substrates working in the 2 GHz – 15 GHz frequency range [1][3][4].

There have been several fabrication routes proposed for diamond-based SAWs: piezoelectric thin film on the nucleation surface of the diamond substrate (this work) [5][6][7], embedding the IDTs either depositing the piezoelectric thin film on the nucleation surface of as-grown diamond substrates[8] or coating the IDT and piezoelectric thin film with a diamond layer grown by chemical vapor deposition (CVD)[9].

Among the most important requirements for SAW based devices on telecommunication technologies are devices with increased performances such as temperature stability and a strong electromechanical coupling coefficient ($K^2$). Thermal stability issues can be tackled by applying thermal engineering, using, for example, compensation layers to optimize the effective thermal expansion coefficient of the heterostructure [10], or using platinum (Pt) as electrode material [11].

However, a strong electromechanical coupling coefficient demands a high piezoelectric $d_{33}$ constant, which thin film polycrystalline piezoelectric materials like aluminum nitride (AlN) and zinc oxide (ZnO) do not provide [12]. New progresses in material engineering have demonstrated that doping these thin film piezoelectric compounds increases their piezoelectric constant [13][14]. Increasing their piezoelectric response, without counterpart compromising other properties for which these polycrystalline materials outstand (e.g. high hardness, wide energy band gap and high thermal conductivity at room temperature), expands their application scope.

The scandium aluminum nitride compound, which has been extensively studied during the last decade, is a representative example of the former.The introduction of scandium (Sc) atoms into the AlN wurtzite-like phase increases the compound piezoelectric $d_{33}$ constant. The maximum increase (~500 %) is provided by a $Sc_{0.43}Al_{0.57}N$ thin film composition [15]. When the intrinsic properties of the ScAlN compound are taken into account, the addition of Sc atoms into the AlN lattice not only alters the $d_{33}$ constant but also reduces its elastic constants, which is reflected on the SAW acoustic velocity [16][17].

In this work, we fabricate surface acoustic devices on scandium aluminum nitride/polycrystalline diamond heterostructures. Highly c-axis oriented ScAlN thin films can be obtained by means of reactive sputtering [18]. The influence of the piezoelectric thin film thickness on the generated Rayleigh and Sezawa resonance frequency modes is assessed with the electrical characterization of the devices. By curve fitting the simulation results of a modified Butterworth Van Dyke (mBVD) model to the electrical measurements, the electromechanical coupling coefficient, the quality factor and the dielectric losses of the fabricated devices are obtained.

## ((2)). Experimental Section

*A.* (1) *Polycrystalline diamond substrate and the $Sc_{0.26}Al_{0.74}N$ thin film synthesis*

Polycrystalline diamond films were synthesized by microwave plasma chemical vapour deposition (MPCVD) on top of 500 µm thick Si (001) substrates. The silicon substrates were cleaned with standard RCA SC1 processes. Following this, they were immersed into an aqueous colloid of diamond nanoparticles under ultrasound, a process known to produce nucleation densities in excess of $10^{11}$ $cm^{-2}$ [19]. These substrates were then rinsed, spun dry and loaded into a Seki 6500 microwave plasma chemical vapour deposition system. Diamond was grown at approximately 0.6 µm/hour at 900 ºC. The gas phase was 478 $H_2$, 20 $CH_4$, 2 $O_2$ at 12000 Pa. The microwave power was 5 kW and the films were grown to 10 µm thick. These films were subsequently polished by a combination of lapping and chemical mechanical polishing [20]. The polished polycrystalline diamond substrates were analysed by means of atomic force microscopy (Veeco Dimension 3100 AFM).

Three different thicknesses of the piezoelectric thin film namely 1700 nm, 2000 nm and 2300 nm have been synthesized on the polycrystalline diamond substrates. The $Sc_{0.26}Al_{0.74}N$ thin films were deposited in a home-built reactive balanced magnetron sputter deposition system. The synthesis, carried out at room temperature, was performed using a 101.6 mm diameter ScAl alloy target (40 wt.% Sc), with a purity of 99.99%. During the deposition, the admixture ratio of the N7.0 process gases, namely argon (Ar) and nitrogen ($N_2$), was kept constant at $Ar/(Ar + N_2) = 25$ %.

The $Sc_{0.26}Al_{0.74}N$ thin films were synthesized with a discharge power of 700 W, a process pressure of 0.53 Pa and a target to substrate distance set to 45 mm. Further information about the $Sc_{0.26}Al_{0.74}N$ thin film synthesis can be found elsewhere[21].The thin film composition, $Sc_{0.26}Al_{0.74}N$, was analysed by means of Rutherford backscattering spectrometry (RBS) at a backscattering angle of 160°.

The presence of the c-axis oriented phase in the synthesized $Sc_{0.26}Al_{0.74}N$ thin film was studied by x-ray diffraction (Phillips X-Pert Pro MRD diffractometer) analysis. θ-2θ scans were first performed in order to determine the $Sc_{0.26}Al_{0.74}N$ thin film texture. ω scans were performed afterwards on the reflection of the wurtzite like phase.

*B. IDT fabrication*

The synthesized $Sc_{0.26}Al_{0.74}N$ thin films were rinsed in acetone at 60 ºC for 5 minutes followed by 5 minutes in a methanol sonication bath. Following this two-solvent cleaning method, the polycrystalline piezoelectric thin films were blown dried with $N_2$ and subjected to an oxygen ($O_2$) plasma (plasmaetch PE-50) cleaning. The ZEP520 resist was spun afterwards. Because of the insulating behaviour of the $Sc_{0.26}Al_{0.74}N$ thin film, as well as of the underlaying polycrystalline diamond layer, an organic anti-static layer (Espacer 300Z, Showa Denko) was spun on top of the ZEP520 resist to avoid charge accumulation during the e-beam lithography process [3].

The resonator interdigital transducer (IDT) was then exposed using a Crestec CABL-9500C e-beam lithography system. In order to remove suspected resist residues, the developed resist was subjected to an $O_2$ plasma. The 350 nm resist thickness was assessed using a KLA Tenkor Alpha Step IQ profilometer.

An e-beam evaporator system (Varian VT 118) was used to metalize the SAW device. The platinum (Pt) target material (99.99%) was placed at a distance between the target and substrate of 45 cm, ensuring a uniform metallization thickness. The 250 nm thick Pt electrodes were evaporated with a 2.5 Å/s rate. Finally, the resist was stripped with N-Methyl-2-pyrrolidone at 80 ºC.

The resonator design (Figure 1) had an IDT periodicity set to $\lambda$=2800 nm and a metallization ratio of 0.5.

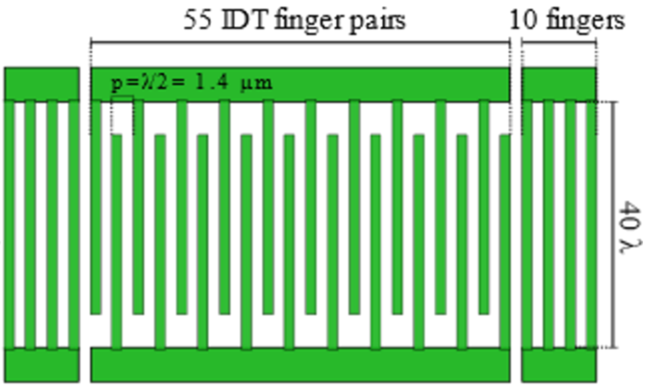


*Figure 1((Figure Caption IDT design*

*C. Frequency analysis*

Standard, 300 µm pitch, ground-source-ground (GSG) probes (Picoprobe 40A; C style adaptor) were connected to a vector network analyser Agilent N5230 A model to electrically characterize the fabricated devices at room temperature. The electrical measurements were carried out using a standard short, open, load, through (SOLT), 50 Ω, one-port calibration. This calibration was performed before each measurement in order to remove systematic errors. The measurement resolution was set to 16001 points in the 1.25 to 4.25 GHz frequency range and the output power set to 0 dBm.

*D. Modified Butterworth Van Dyke model*

Simulations with a modified Butterworth Van Dyke (mBVD) model (**Figure 2**), implemented in the Keysight advanced design system (ADS), were employed to curve fitting the electrical response of the fabricated devices. The resistor $R_s$ represents the ohmic loss from the IDT fingers and bonding pads, $C_0$ is the substrate plate capacitance and $R_0$ represents the dielectric loss of the heterostructure. The Rayleigh and Sezawa resonance frequency modes are modelled using a series branch of motional inductance $L_m$, capacitance $C_m$, and resistance $R_m$ for each particular mode. The $L_m$, $C_m$, and $R_m$ values corresponding to the Rayleigh and Sezawa resonance frequency modes can be found in Table 1.

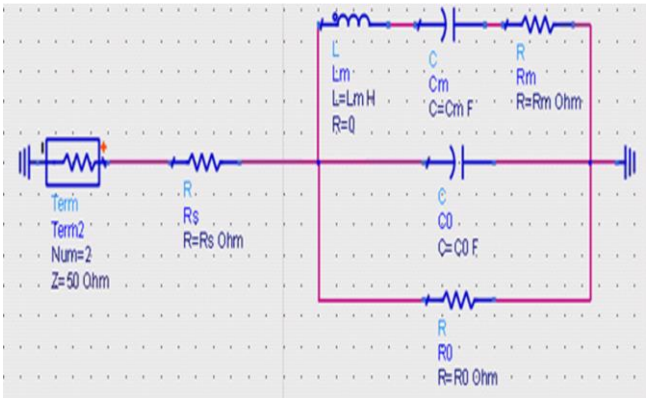


**Figure 2.** ((Figure Caption. Equivalent one-port parallel mBVD circuit model))

## 2. Results

A large substrate roughness complicates the promotion of highly c-axis ordered ScAlN thin film synthesis [22]. Additionally, the most relevant loss mechanism for a SAW propagating through polycrystalline materials is scattering due to the inhomogeneities within the synthesized thin films [23]. For these reasons, the polished polycrystalline diamond substrates were analysed by AFM. The root mean squared roughness ($R_{RMS}$) value (0.59 nm in a square area of 5x5 $\mu m^2$) report the low surface roughness of the polished polycrystalline diamond film (see supplementary material, Figure S1).

The ω scan FWHM values of the 1700 nm, 2000 nm, 2300 nm ScAlN thick ScAlN thin films are 2.58º, 2.98º, and 2.65º respectively, indicating that the piezoelectric thin film is highly c-axis textured (see supplementary material, Figure S2). These values are comparable to those reported for ScAlN thin films using synthesis temperatures above 400 ºC on Si (100) substrates [24][25].

The electrical characterization (**Figure 3**) shows that several resonance frequency modes are generated in the SAW resonator fabricated in the heterostructure comprising a 2000 nm thick ScAlN thin film. Among these propagating resonance frequency modes, the reflection coefficient (**Figure 3 A**) above -50 dB of the Sezawa resonance frequency mode (2.654 GHz) outstands when compared to the Rayleigh resonance frequency mode one (1.579 GHz) and those reflection coefficients of the harmonics propagating above 3 GHz.

There is a necessary piezoelectric thin film layer of about 0.2 λ for the Sezawa resonance frequency mode to propagate unattenuated [2]. However, this is not the only condition for achieving a large reflection coefficient. For that, the dielectric properties of the $Sc_{0.26}Al_{0.74}N$ thin film together with the IDT design were thoroughly considered for matching the impedance to 50 Ω.

The admittance characteristic (**Figure 3 B**) confirms that there are no transverse mode resonances, indicating that no spurious resonances are generated close to the Rayleigh and

Sezawa resonance frequencies [23]. Furthermore, the close fitting between the mBVD model simulation with the experimental results validates the parameter extraction and their analysis in this work. Additionally, the series ($f_s$) (Equation (2))and parallel ($f_p$) (Equation (3)) resonance frequencies of the Rayleigh ($^o$) and Sezawa ($^1$) resonance frequency modes can be employed for obtaining the experimental SAW velocity (see below).

$$f_s = 1/2\pi\sqrt{L_m C_m} \quad (2)$$

$$f_p = 1/2\pi\sqrt{L_m C_m C_0 / (C_m + C_0)} \quad (3)$$

Comparing the electrical performance of our devices with those reported by Fujii et al. [1], we have observed a displacement towards ~0.02 S of the conductance base (not shown) indicating our device has a larger substrate dielectric loss. According to them, one of the reasons for the high substrate dielectric loss is the polycrystalline diamond employed in this work heterostructures.

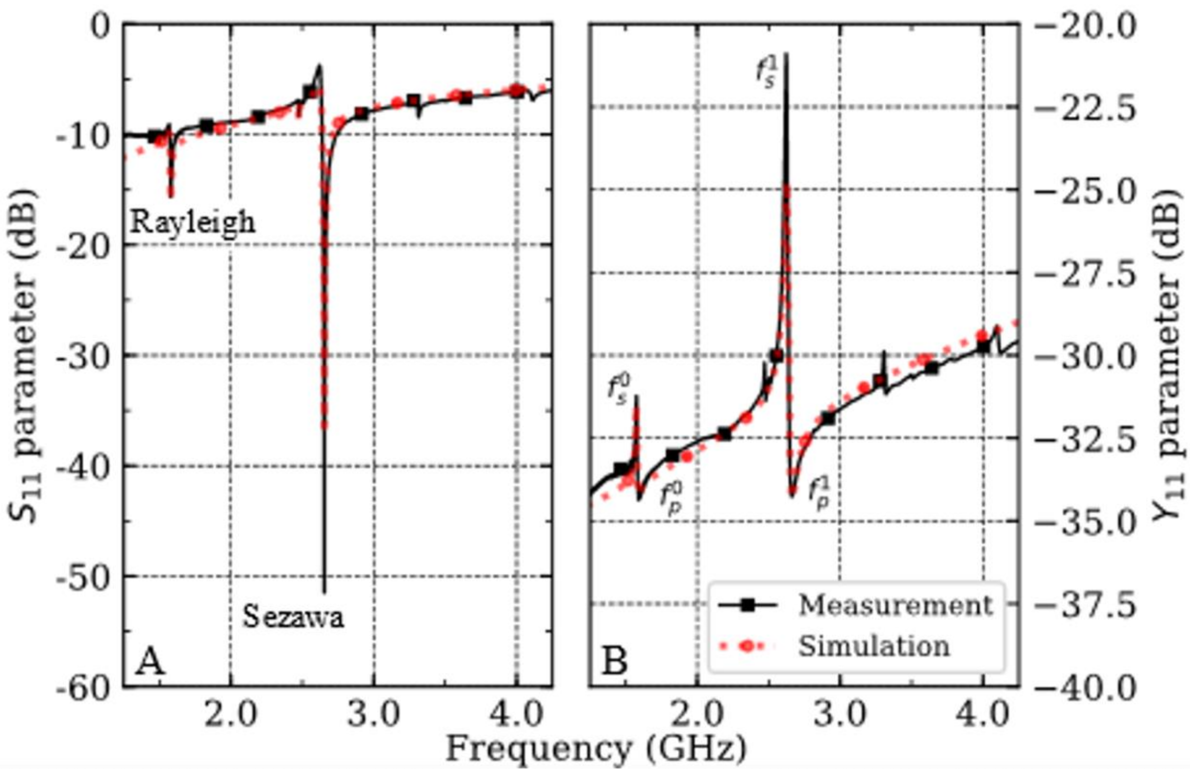


**Figure 3** ((Figure Caption. Electrical characterization and mBVD model simulation result (dotted line) of the one-port SAW resonator with a 250 nm Pt/2000 nm $Sc_{0.26}Al_{0.74}N$/polycrystalline-diamond layered structure. A) Reflection coefficient ($S_{11}$ parameter) B) Admittance characteristics ($Y_{11}$ parameter)))

The shift that the ScAlN thin film thickness causes on the propagating Rayleigh and Sezawa mode resonance frequencies is remarkable. This is observed in the electrical characterization of the one-port resonators fabricated on heterostructures with a varying piezoelectric thin film thickness (**Figure 4**). The effective SAW velocity is determined by the predominant propagation of the generated wave (λ=2800 nm), either through the $Sc_{0.26}Al_{0.74}N$ thin film or through the polycrystalline diamond substrate [23]. This is the reason behind the different frequency shifts experienced by the propagating Rayleigh and Sezawa modes.

The Smith chart (**Figure 4** (inset)) depicts the impedance matching of the Sezawa resonance frequency mode with the characteristic impedance (50 Ω). The predominant capacitive behavior of the fabricated SAW resonators becomes apparent in all three thicknesses under study.

The electrical performance of the fabricated SAW devices is comparable to those previously reported for the ScAlN/diamond heterostructures. However, their reflection coefficient in the Rayleigh and Sezawa resonance modes are, to the best of our knowledge, the largest reported in the ScAlN thin film SAW technology [4][17][26].

The three ScAlN thin film thicknesses were selected after studying the dispersion curves reported by Hashimoto et al. [4][27], for ScAlN thin film/polycrystalline diamond heterostructures. With these thicknesses, the frequency range of the generated Sezawa modes is targeted to be between 2.4 GHz to 2.7 GHz, providing high electromechanical coupling coefficient.

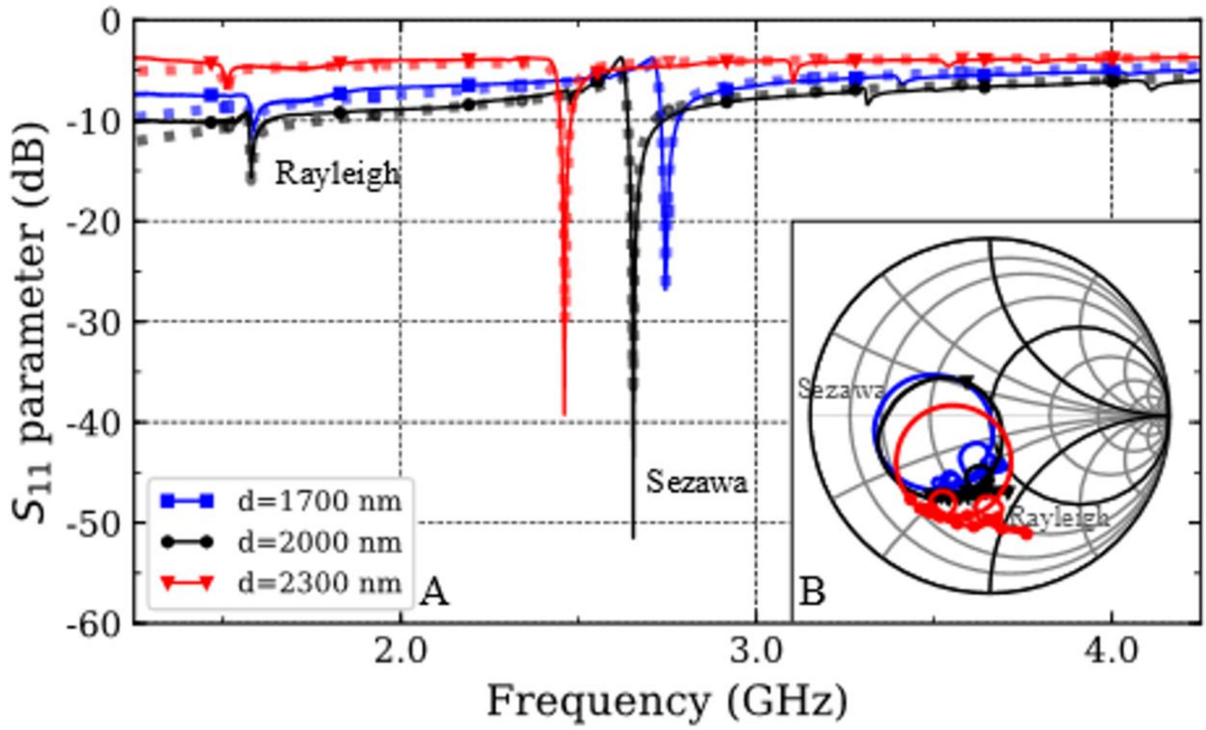


**Figure 4.** ((Figure Caption. Electrical characterization and mBVD model simulation results (dotted lines) of 250 nm Pt/$Sc_{0.26}Al_{0.74}N$ /polycrystalline-diamond heterostructures with different ScAlN thin film thickness. The reflection coefficient shows the Rayleigh and Sezawa propagation modes together with second and third resonance modes. (inset) Device impedance Smith chart. d stands for the $Sc_{0.26}Al_{0.74}N$ thin film thickness))

In the following, the thin film thickness ratio (d/λ) is employed for a better comparison between the heterostructures fabricated in this work and those found in the literature. It relates the piezoelectric thin film thickness (d) and the IDT wavelength (λ).

The series and ($f_s$) and parallel ($f_p$) resonance frequencies for the Rayleigh and Sezawa modes are employed for computing the effective SAW velocity (Equation (4)) [12][26].

$$v_{eff} = \lambda(f_p - f_s)/2 \quad (4)$$

As commented above, the effective SAW velocity (**Figure 5**) is determined by the predominant propagation of the SAW through the heterostructure layers. Therefore, the SAW velocity resembles the acoustic velocity of the $Sc_{0.26}Al_{0.74}N$ thin film when the SAW is mainly confined within the piezoelectric layer. In other words, when the d/λ ratio is close to 1, a larger fraction of the generated SAW propagates through the piezoelectric thin film approaching the intrinsic acoustic speed of the $Sc_{0.26}Al_{0.74}N$ thin film.

However, as the piezoelectric thin film thickness increases, the effective SAW velocity corresponding to the Sezawa and Rayleigh modes are altered differently. The effective SAW velocity of the Rayleigh mode experiences a slight deceleration (5 %) whereas the Sezawa mode speed undergoes a steeper deceleration (11 %).

This behavior agrees with the dispersion curves reported by Hashimoto et al. [4][27] which show how, within the d/λ range used in this work, the propagation velocity of the Rayleigh mode approaches the characteristic velocity of the piezoelectric ScAlN compound whereas the Sezawa mode velocity is affected by the increase of the d/λ ratio.

The propagation speeds presented here are slightly larger than those previously reported [4][27]. As commented in the introduction, the acoustic velocity depends on the elasticity constants and density of the material the wave propagates through. The discrepancy between the simulated and our experimentally obtained effective SAW velocities arises because of the decrease of the $Sc_xAl_{1-x}N$ compound elasticity constants due to the higher scandium concentration (x) [16]. The values employed by Hashimoto et al. [4][27] correspond to a thin film composition of $Sc_{0.40}Al_{0.60}N$ whereas, in this work, the Rutherford backscattering spectrometry analysis report a thin film composition of $Sc_{0.26}Al_{0.74}N$.

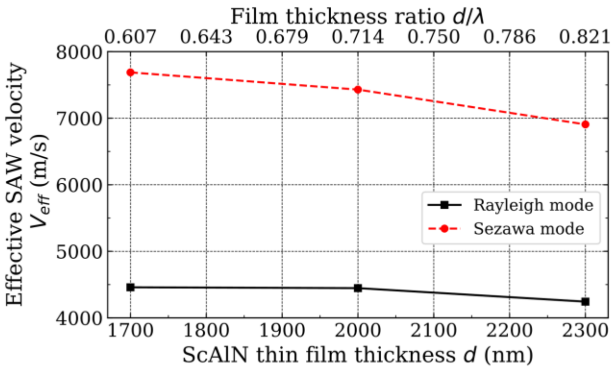


**Figure 5.** ((Figure Caption. Effective SAW velocity of the generated Rayleigh and Sezawa modes in the $Sc_{0.26}Al_{0.74}N$ /polycrystalline-diamond heterostructure with different piezoelectric thin film thicknesses. λ=2800 nm))

According to the mBVD model simulation results (**Table 1**) the fabricated SAW resonators possess relatively high ohmic losses (Rs) caused by the thick Pt electrodes. Although this metal is more resistive than other metals usually employed in microfabrication technologies such as Au or Cu, it is extensively used for high temperature applications due its high thermal stability [11]. Several authors have modelled FBAR resonators on AlN and ScAlN thin films [28][29]. However, a proper comparison with those values cannot be performed for the different device technologies.

**Table 1** ((Table Caption. ADS simulation results))

| | **ScAlN thin film thickness [nm]** | **$f_s$ [GHz]** | **$f_p$ [GHz]** | **$R_s$ [Ω]** | **$C_0$ [F] ($\cdot 10^{-12}$)** | **$R_0$ [Ω]** | **$L_m$ [H] ($\cdot 10^{-06}$)** | **$C_m$ [F] ($\cdot 10^{-14}$)** | **$R_m$ [Ω]** | **tanδ** |
|---|---|---|---|---|---|---|---|---|---|---|
| **Rayleigh mode** | 1700 | 1.57 | 1.59 | 7.90 | 1.57 | 67.6 | 1.70 | 0.60 | 170 | 0.86 |
| | 2000 | 1.57 | 1.58 | 11.8 | 1.61 | 54.9 | 1.61 | 0.63 | 83.7 | 0.94 |
| | 2300 | 1.50 | 1.51 | 9.50 | 1.89 | 140 | 1.71 | 0.65 | 184 | 0.37 |
| **Sezawa mode** | 1700 | 2.71 | 2.75 | 7.90 | 1.57 | 67.6 | 0.10 | 3.20 | 8.27 | 0.55 |
| | 2000 | 2.62 | 2.66 | 11.8 | 1.61 | 54.9 | 0.09 | 3.82 | 8.60 | 0.68 |
| | 2300 | 2.43 | 2.47 | 9.50 | 1.89 | 140 | 0.11 | 3.62 | 16.92 | 0.24 |

The substrate permittivity is a significant parameter in the device design, as it determines the impedance of the interdigital transducer. This parameter is closely related to the substrate dielectric loss (Equation (5))which is related to the material properties within the heterostructure [30].

$$\tan\delta = (2\pi f_p C_0 R_0)^{-1} \tag{5}$$

The dependency of the tan $\delta$ value with the modelled dielectric loss ($R_0$) takes on importance in the heterostructure comprising a ScAlN thin film thickness of 2300 nm. This device presents the lower tan $\delta$ value for the Rayleigh and Sezawa modes among the three fabricated devices.

Larger effective electromechanical coupling coefficients (Equation (6)) are obtained for the Sezawa mode than for the Rayleigh mode (**Figure 6**) [4][27].

$$K_{eff}^2 = \left(\frac{\pi^2}{8}\right)\left(\frac{C_m}{C_0}\right)\left(\frac{C_0 - C_m}{C_0}\right) \tag{6}$$

The largest effective electromechanical coupling coefficient for the Rayleigh (0.48 %) and the Sezawa (2.86 %) modes are obtained for a thin film thickness ratio of 0.714. On the other hand, the smallest Rayleigh (0.42 %) and Sezawa (2.32 %) mode $K_{eff}^2$ coefficients correspond to the heterostructure with a 2300 nm thick ScAlN thin film.

Within the d/λ range employed in this work, there is a larger variation in the Sezawa mode $K_{eff}^2$ coefficients (23 %) than for those of the propagating Rayleigh mode (14 %). The former is in agreement with the electromechanical coupling coefficient dispersion curves reported in [4] and [27]. However, while the Rayleigh mode effective electromechanical coupling coefficients are in agreement with those reported in the literature [4][27], the calculated Sezawa mode $K_{eff}^2$ coefficients are reduced by a 40 % as compared to those of the simulated dispersion curves. The reason behind this is the mismatch between the material constants employed for the simulation (a $Sc_{0.40}Al_{0.60}N$ composition) and the ones of the synthesized $Sc_{0.26}Al_{0.74}N$ thin film together with the device IDT design.

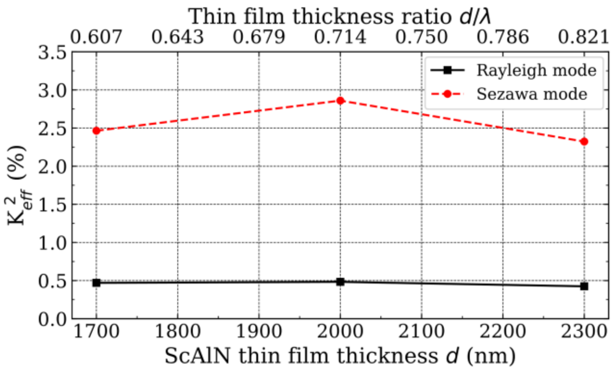


**Figure 6.** ((Figure Caption. Variation of the Rayleigh and Sezawa mode effective electromechanical coupling coefficient ($K_{eff}^2$) with ScAlN thin film thickness and thin film thickness ratio. λ=2800 nm))

The quality factor (Equation (7)) of a SAW resonator depends on the device design and the properties of the materials within the heterostructure.

$$(Q_s = 2\pi f_s \frac{L_m}{R_m}) \qquad (7)$$

Fujii et al. [1] report on the influence that the grain boundaries of several polycrystalline substrates have on the admittance characteristics of SAW devices. Using single-crystal diamond substrates reduce the propagation losses which in turns increases the quality factor. Therefore, in heterostructures comprising a polycrystalline diamond layer, the quality factor is limited by the scattering from its grain boundaries and the substrate dielectric loss $\tan\delta$ [1]. Because of the linear proportionality of the quality factor with the series resonance frequency the Sezawa mode $Q_s$ of the fabricated devices in this work is larger than those of the Rayleigh mode ones (**Figure 7**). The quality factor of the propagating Sezawa mode decreases linearly, as the $Sc_{0.26}Al_{0.74}N$ thin film thickness increases from 1700 nm to 2300 nm, by a 50 %. On the other hand, the largest quality factor (166.8) among the propagating Rayleigh mode corresponds to the heterostructure with a 2000 nm thick ScAlN thin film. As commented above, the series branches of motional inductance, capacitance, and resistance represent the resonating wave modes in the mBVD model. After the curve fitting procedure of the modified Butterworth Van Dyke model, different inductance and resistance values are obtained in the series branches that correspond to the Rayleigh and Sezawa modes. The Rayleigh mode Rm value for the 2000 nm resonator is approximately half the value corresponding to the 1700 nm and 2300 nm resonator. Due to this, the Rayleigh mode quality factor does not show the linear dependency shown by the Sezawa mode quality factor.

The quality factors obtained in this work are above those previously reported values for SAW devices fabricated on $Sc_{0.27}Al_{0.73}N$/Si (100) heterostructures [17], indicating that the heterostructure presented in this work is a promising device configuration for future applications in the SAW technologies.

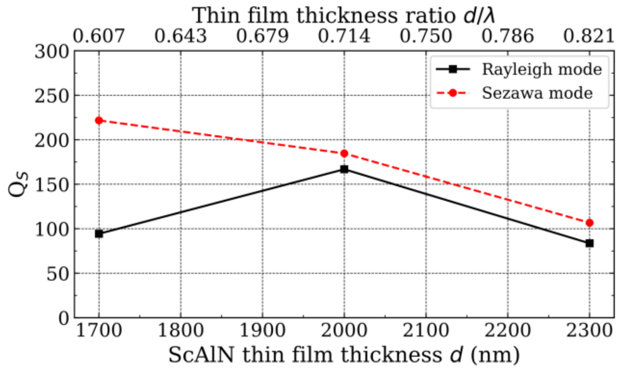


**Figure 7.** ((Figure Caption. Variation of the Rayleigh and Sezawa quality factor ($Q_S$) with the $Sc_{0.26}Al_{0.74}N$ thin film thickness. λ=2800 nm))

**((4)). Conclusion**

Highly c-axis oriented $Sc_{0.26}Al_{0.74}N$ thin films were synthesized on polycrystalline diamond substrates. Using e-beam lithography, one-port SAW resonators were fabricated on three heterostructures comprising a polycrystalline diamond substrate, a scandium aluminium nitride thin film and platinum electrodes. The piezoelectric thin film thickness was varied in these three heterostructures and the electrical response of the fabricated one-port resonators analysed. In these devices a remarkable reflection coefficient at the Sezawa resonance frequency mode is observed in the fabricated SAW devices. The corresponding effective electromechanical coupling coefficient factor ($K_{eff}^2$), the quality factor ($Q_s$) and the dielectric loss (tanδ) for the Rayleigh and the Sezawa resonance modes are computed from the curve fitting of the modified Butterworth Van Dyke model simulation implemented in the ADS design tool.

A slight variation of the Rayleigh mode electromechanical coupling coefficient $K_{eff}^2$ is observed. This is in agreement with the dispersion curves that have been previously reported for the ScAlN thin film/diamond heterostructure. On the other hand, the Sezawa mode electromechanical coupling coefficient is largely influenced by the ratio between the piezoelectric thin film thickness and the designed IDT wavelength. However, the Sezawa mode $K_{eff}^2$coefficients obtained here are a 40% below those previously reported from the simulations. This is due to the different thin film compositions employed. Whereas in this work the Rutherford backscattering spectrometry analysis report a $Sc_{0.26}Al_{0.74}N$ thin film composition, the simulations are performed for a $Sc_{0.40}Al_{0.60}N$ thin film [4][27].

The quality factors ($Q_s$) obtained in this work are within those previously reported for IDT/ScAlN/polycrystalline-diamond heterostructures and are largely related to the device design.

According to the obtained SAW characteristics, the presented $Sc_{0.26}Al_{0.74}N$ thin film based heterostructures are a promising candidate for fabricating SAW devices. They are not only a feasible candidate for the 5G telecommunication products but also in SAW based sensory applications.

**Acknowledgements**

-

Received: ((will be filled in by the editorial staff))
Revised: ((will be filled in by the editorial staff))
Published online: ((will be filled in by the editorial staff))

**References**

[1] S. Fujii, T. Odawara, H. Yamada, T. Omori, K. Hashimoto, H. Torii, H. Umezawa, S. Shikata, *IEEE Trans. Ultrason. Ferroelectr. Freq. Control* **2013**, *60*, 986.

[2] G. W. Farnell, E. L. Adler, in *Phys. Acoust.*, Academic Press, INC., **1972**, pp. 35–127.

[3] G. F. Iriarte, J. G. Rodriguez-Madrid, F. Calle, *J. Mater. Process. Technol.* **2012**, *212*, 707.

[4] K. Hashimoto, T. Fujii, S. Sato, T. Omori, Changjun Ahn, A. Teshigahara, K. Kano, H. Umezawa, S. Shikata, in *2012 IEEE Int. Ultrason. Symp.*, IEEE, **2012**, pp. 1–4.

[5] V. Mortet, O. Elmazria, M. Nesladek, M. B. Assouar, G. Vanhoyland, J. D'Haen, M. D'Olieslaeger, P. Alnot, *Appl. Phys. Lett.* **2002**, *81*, 1720.

[6] T. Lamara, M. Belmahi, O. Elmazria, L. Le Brizoual, J. Bougdira, M. Rémy, P. Alnot, *Diam. Relat. Mater.* **2004**, *13*, 581.

[7] J. LIU, Y. XIA, L. WANG, Q. SU, P. ZHAO, R. XU, H. PENG, W. SHI, *Trans. Nonferrous Met. Soc. China* **2006**, *16*, s298.

[8] B. Bi, W.-S. Huang, J. Asmussen, B. Golding, *Diam. Relat. Mater.* **2002**, *11*, 677.

[9] D. Mukherjee, F. J. Oliveira, R. F. Silva, J. F. Carreira, L. Rino, M. R. Correia, S. Z. Rotter, L. N. Alves, J. C. Mendes, *Phys. status solidi* **2016**, *13*, 53.

[10] J. H. Kuypers, Chih-Ming Lin, G. Vigevani, A. P. Pisano, in *2008 IEEE Int. Freq. Control Symp.*, IEEE, **2008**, pp. 240–249.

[11] M. S. Lozano, Z. Chen, O. A. Williams, G. F. Iriarte, *Smart Mater. Struct.* **2018**, *27*, 075015.

[12] R. Ro, R. Lee, Z.-X. Lin, C.-C. Sung, Y.-F. Chiang, S. Wu, *Thin Solid Films* **2013**, *529*, 470.

[13] C. Tholander, F. Tasnádi, I. A. Abrikosov, L. Hultman, J. Birch, B. Alling, *Phys. Rev. B* **2015**, *92*, 174119.

[14] A. Žukauskaitė, G. Wingqvist, J. Palisaitis, J. Jensen, P. O. Å. Persson, R. Matloub, P. Muralt, Y. Kim, J. Birch, L. Hultman, *J. Appl. Phys.* **2012**, *111*, 093527.

[15] M. Akiyama, T. Kamohara, K. Kano, A. Teshigahara, Y. Takeuchi, N. Kawahara, *Adv. Mater.* **2009**, *21*, 593.

[16] M. A. Caro, S. Zhang, T. Riekkinen, M. Ylilammi, M. A. Moram, O. Lopez-Acevedo, J. Molarius, T. Laurila, *J. Phys. Condens. Matter* **2015**, *27*, 245901.

[17] W. Wang, P. M. Mayrhofer, X. He, M. Gillinger, Z. Ye, X. Wang, A. Bittner, U. Schmid, J. K. Luo, *Appl. Phys. Lett.* **2014**, *105*, 133502.

[18] M. Akiyama, T. Tabaru, K. Nishikubo, A. Teshigahara, K. Kano, *J. Ceram. Soc. Japan* **2010**, *118*, 1166.

[19] J. Hees, A. Kriele, O. A. Williams, *Chem. Phys. Lett.* **2011**, *509*, 12.

[20] E. L. H. Thomas, G. W. Nelson, S. Mandal, J. S. Foord, O. A. Williams, *Carbon N. Y.* **2014**, *68*, 473.

[21] M. Sinusía Lozano, A. Pérez-Campos, M. Reusch, L. Kirste, T. Fuchs, A. Žukauskaitė, Z. Chen, G. F. Iriarte, *Mater. Res. Express* **2018**, *5*, 036407.

[22] G. F. Iriarte, J. G. Rodríguez, F. Calle, *Mater. Res. Bull.* **2010**, *45*, 1039.

[23] K. Hashimoto, *Surface Acoustic Wave Devices in Telecommunications*, Springer Berlin Heidelberg, Berlin, Heidelberg, **2000**.

[24] M. Akiyama, K. Kano, A. Teshigahara, *Appl. Phys. Lett.* **2009**, *95*, 162107.

[25] Y. Lu, M. Reusch, N. Kurz, A. Ding, T. Christoph, L. Kirste, V. Lebedev, A.

Žukauskaitė, *Phys. status solidi* **2017**, *1700559*, 1700559.

[26] Q. Zhang, T. Han, J. Chen, W. Wang, K. Hashimoto, *Diam. Relat. Mater.* **2015**, *58*, 31.

[27] K. Hashimoto, S. Sato, A. Teshigahara, T. Nakamura, K. Kano, *IEEE Trans. Ultrason. Ferroelectr. Freq. Control* **2013**, *60*, 637.

[28] T. Yokoyama, Y. Iwazaki, Y. Onda, T. Nishihara, Y. Sasajima, M. Ueda, *IEEE Trans. Ultrason. Ferroelectr. Freq. Control* **2015**, *62*, 1007.

[29] M. Moreira, J. Bjurström, I. Katardjev, V. Yantchev, *Vacuum* **2011**, *86*, 23.

[30] R. Matloub, A. Artieda, C. Sandu, E. Milyutin, P. Muralt, *Appl. Phys. Lett.* **2011**, *99*, 092903.

**Figure 1.** ((Figure Caption. IDT design))

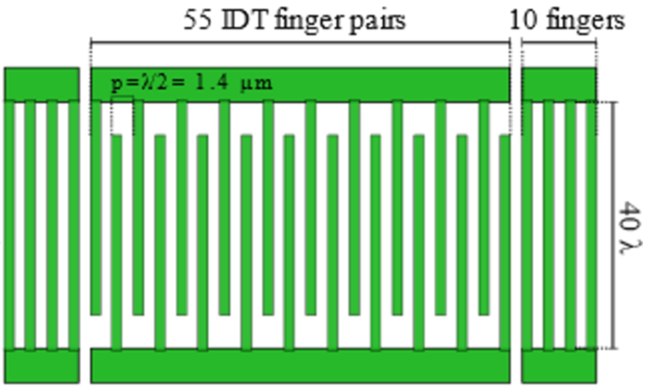

**Figure 2.** ((Figure Caption. Equivalent one-port parallel mBVD circuit model))

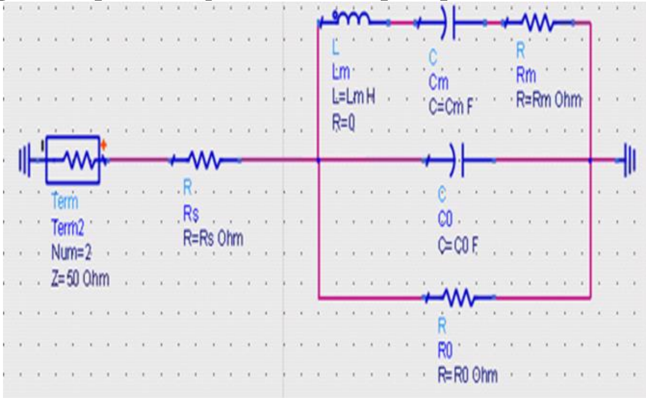

**Figure 3.** ((Figure Caption. Electrical characterization and mBVD model simulation result (dotted line) of the one-port SAW resonator with a 250 nm Pt/2000 nm $Sc_{0.26}Al_{0.74}N$/polycrystalline-diamond layered structure. A) Reflection coefficient ($S_{11}$ parameter) B) Admittance characteristics ($Y_{11}$ parameter)))

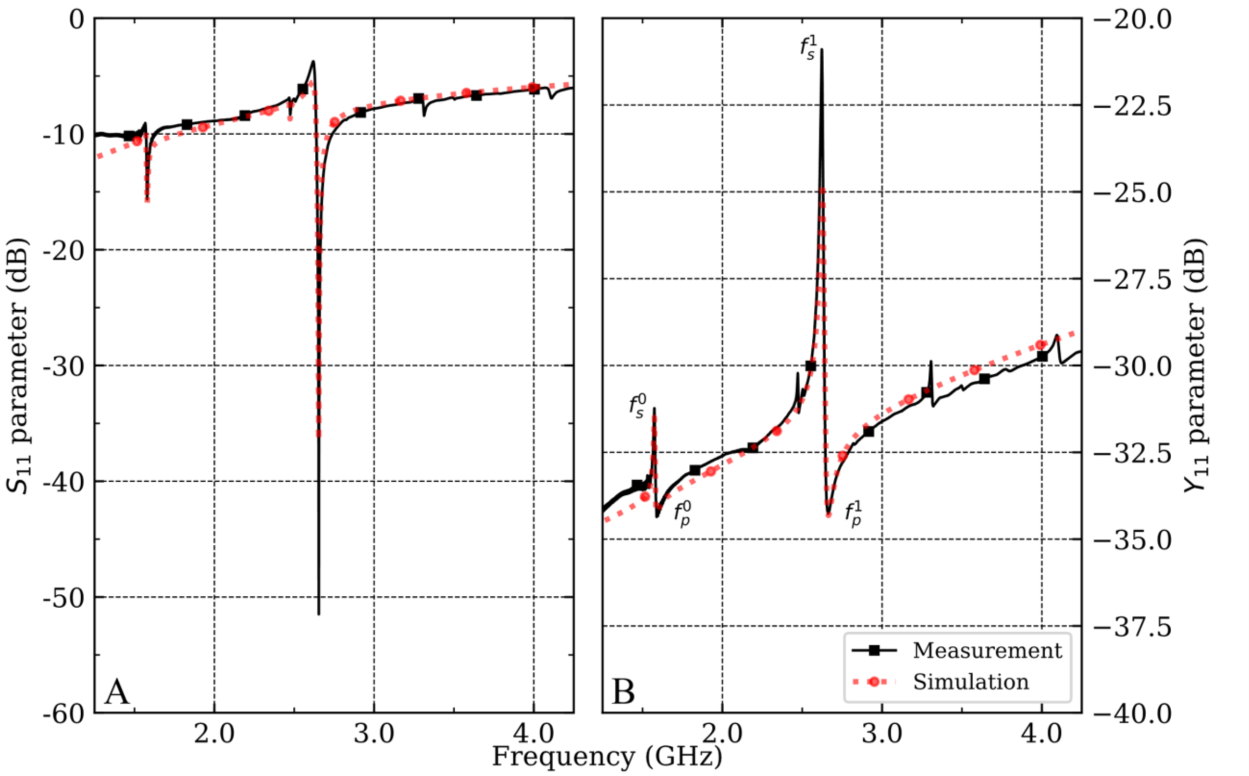

**Figure 4.** ((Figure Caption. Electrical characterization and mBVD model simulation results (dotted lines) of 250 nm Pt/$Sc_{0.26}Al_{0.74}N$ /polycrystalline-diamond heterostructures with different ScAlN thin film thickness. The reflection coefficient shows the Rayleigh and Sezawa propagation modes together with second and third resonance modes. (inset) Device impedance Smith chart. d stands for the $Sc_{0.26}Al_{0.74}N$ thin film thickness))

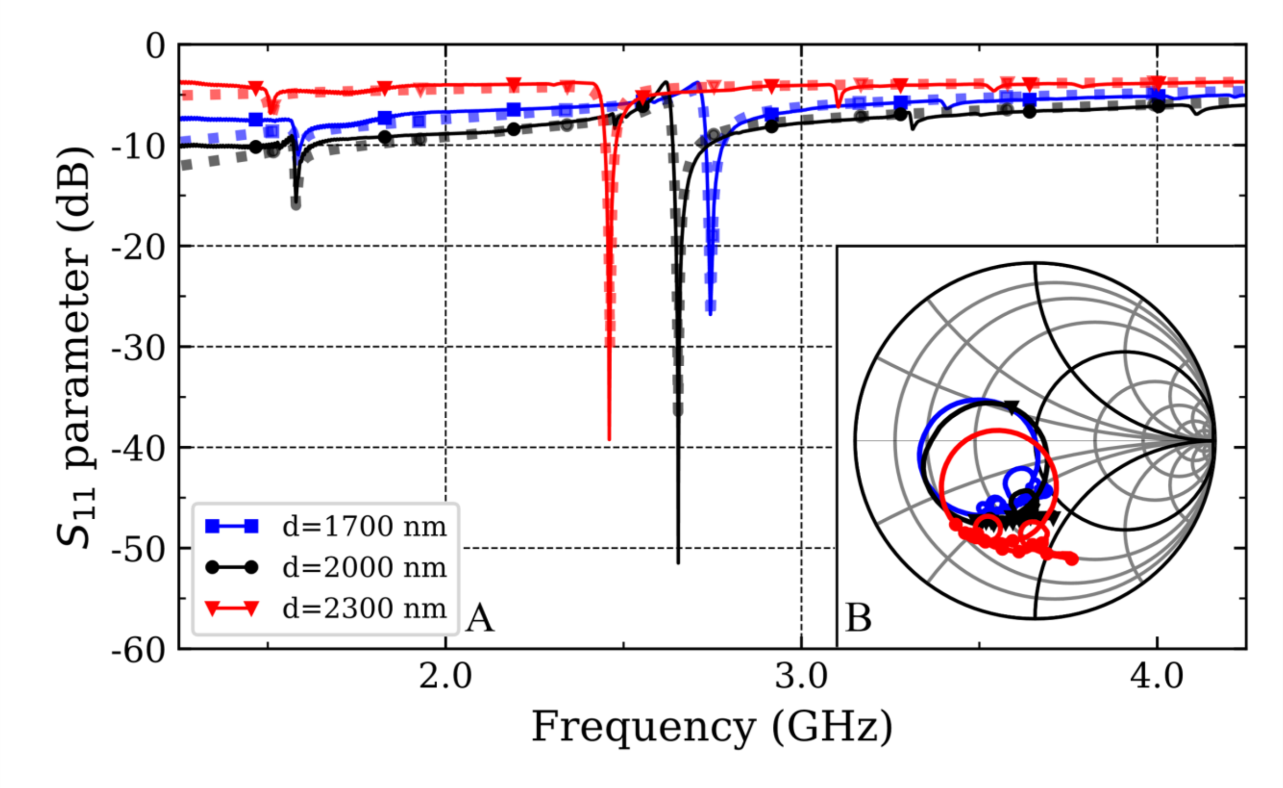

**Figure 5.** ((Figure Caption. Effective SAW velocity of the generated Rayleigh and Sezawa modes in the $Sc_{0.26}Al_{0.74}N$ /polycrystalline-diamond heterostructure with different piezoelectric thin film thicknesses. λ=2800 nm))

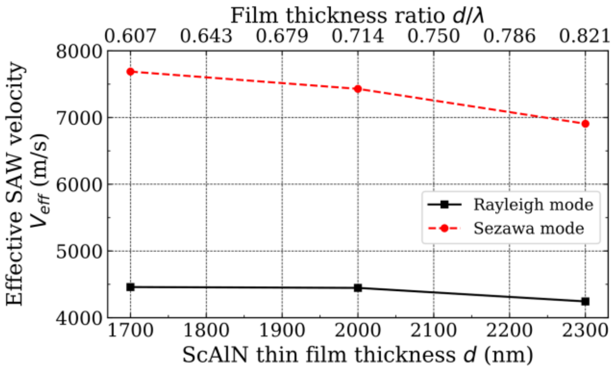

**Figure 6.** ((Figure Caption. Variation of the Rayleigh and Sezawa mode effective electromechanical coupling coefficient ($K_{eff}^2$) with ScAlN thin film thickness and thin film thickness ratio. λ=2800 nm))

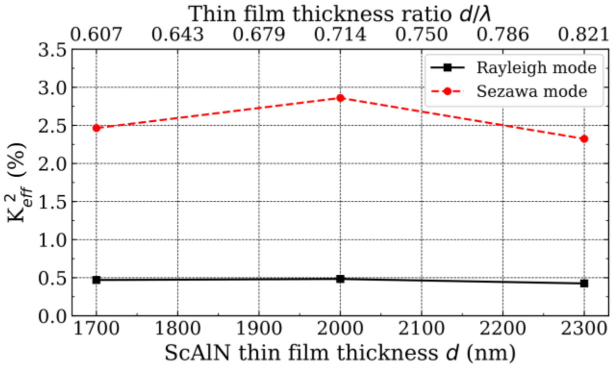

**Figure 7.** ((Figure Caption. Variation of the Rayleigh and Sezawa quality factor ($Q_S$) with the $Sc_{0.26}Al_{0.74}N$ thin film thickness. λ=2800 nm))

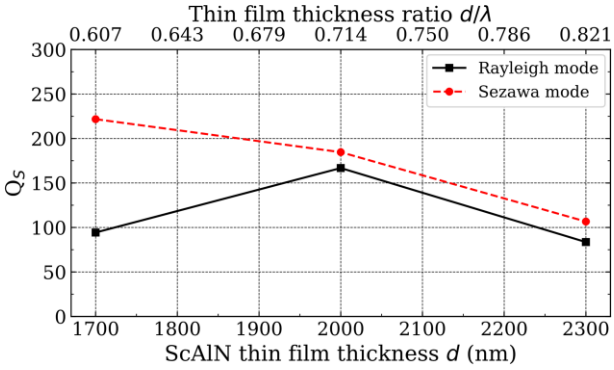

**Table 1** ((Table Caption. ADS simulation results))

| | ScAlN thin film thickness [nm] | $f_s$ [GHz] | $f_p$ [GHz] | $R_s$ [Ω] | $C_0$ [F] ($\cdot 10^{-12}$) | $R_0$ [Ω] | $L_m$ [H] ($\cdot 10^{-06}$) | $C_m$ [F] ($\cdot 10^{-14}$) | $R_m$ [Ω] | tanδ |
|---|---|---|---|---|---|---|---|---|---|---|
| **Rayleigh mode** | 1700 | 1.57 | 1.59 | 7.90 | 1.57 | 67.6 | 1.70 | 0.60 | 170 | 0.86 |
| | 2000 | 1.57 | 1.58 | 11.8 | 1.61 | 54.9 | 1.61 | 0.63 | 83.7 | 0.94 |
| | 2300 | 1.50 | 1.51 | 9.50 | 1.89 | 140 | 1.71 | 0.65 | 184 | 0.37 |
| **Sezawa mode** | 1700 | 2.71 | 2.75 | 7.90 | 1.57 | 67.6 | 0.10 | 3.20 | 8.27 | 0.55 |
| | 2000 | 2.62 | 2.66 | 11.8 | 1.61 | 54.9 | 0.09 | 3.82 | 8.60 | 0.68 |
| | 2300 | 2.43 | 2.47 | 9.50 | 1.89 | 140 | 0.11 | 3.62 | 16.92 | 0.24 |

**Table of contents**

This work studies the characteristics of a novel piezoelectric compound in devices within the scope of their use in the 5G telecommunication industry.

**Keyword** ((5G))

*Miguel Sinusía Lozano, Zhuohui Chen, Oliver A. Williams, Gonzalo F. Iriarte**

**Title** Giant reflection coefficient on $Sc_{0.26}Al_{0.74}N$ /polycrystalline-diamond SAW resonators

ToC figure ((110 mm broad × 20 mm high.))